Supplementary Information for

Li-III-VI_2 bilayers for efficient photocatalytic overall water splitting: The role of intrinsic electric field

Yingcai Fan[1,2], Xiaohan, Song[1], Siyun Qi[1], Xikui Ma[1], Mingwen Zhao[1*]

[1] *School of Physics, Shandong University, Jinan, Shandong, China*

[2] *School of Information and Electronic Engineering, Shandong Technology and Business University, Yantai, Shandong, China*

To whom correspondence should be addressed.

[*]Email: zmw@sdu.edu.cn (M. Zhao).

33 pages, 3 text, 8 table, 19 figures

Text S1. The strategy of determining E for calculating the STH efficiency

In this work, we calculate the values of *E* by introducing cocatalysts, which has been proved to be an efficient method to reducing the needed overpotentials for water splitting[1, 2]. The previous works[3, 4] shown that the needed overpotentials of OER cocatalysts for some oxides of Ir, Ni, Fe, Co, etc., are below 0.5 eV and that of HER cocatalyst for Pt is below 0.1 eV. Considering the energy loss during carrier migration between different materials, the required overpotentials for OER and HER are assumed to be 0.6 and 0.2 eV, respectively. Then, *E* is determined by[1]

$$E = \begin{cases} E_g, (\Delta E_1 \geq 0.6 \text{ eV}, \Delta E_2 \geq 0.2 \text{ eV}) \\ E_g + 0.6 - \Delta E_1, (\Delta E_1 < 0.6 \text{ eV}, \Delta E_2 \geq 0.2 \text{ eV}) \\ E_g + 0.2 - \Delta E_2, (\Delta E_1 \geq 0.6 \text{ eV}, \Delta E_2 < 0.2 \text{ eV}) \\ E_g + 0.8 - \Delta E_1 - \Delta E_2, (\Delta E_1 < 0.6 \text{ eV}, \Delta E_2 < 0.2 \text{ eV}) \end{cases}$$

Text S2. Computational Method of Carrier Mobility

We evaluated the carrier mobility by using a phonon-limited scattering model based on the following expression[5]:

$$\mu_{2D} = \frac{e\hbar^3 C_{2D}}{\kappa_B T m_i^* m_d E_i^2}$$

where the carrier mobility μ_{2D} depends on the elastic modulus C_{2D}, effective mass m^*, and deformation potential constant E_i. In addition, e, $\hbar$, k_B, and T are the electron charge, reduced Planck constant, Boltzmann constant, and the temperature T was set at 300 K. Herein, the elastic modulus C_{2D} is defined as $C_{2D} = (\partial^2(E - E_0)/\,\partial\varepsilon^2)/S_0$, where $E - E_0$ is the total energy shift with respect to the applied uniaxial strain ε and S_0 is the equilibrium area of the optimized 2D structure. The carrier effective mass m_i^* (i = h for holes and i = e for electrons) was obtained via $m^* = \hbar^2(\partial^2 E/\partial k^2)$. The term m_d is the average effective mass given as $m_d = \sqrt{m_x^* m_y^*}$. The deformation potential constant E_i is derived from $E_i = \partial E_{edge}/\partial\varepsilon$, where E_{edge} is the band edge energy of the CBM for electrons and VBM for holes induced by the strain ε.

Text S3. The strategy of free energy change for OER and HER

To compute the free energy change (ΔG) in the hydrogen reduction and water oxidation reactions, we adopted the method developed by Nørskov et al, according to which the ΔG of an electrochemical reaction is computed as[6-9]:

$$\Delta G = \Delta E + \Delta E_{ZPE} - T\Delta S$$

where ΔE is the DFT computed reaction (electronic) energy, ΔE_{ZPE} and ΔS are the zero-point energy difference and the entropy difference between the adsorbed state and the gas phase, respectively, and T is the system temperature (298 K, in our work). For each system, its E_{zpe} for each adsorbate and free molecules can be calculated by summing vibrational frequencies over all normal modes ν ($E_{zpe} = 1/2\Sigma\hbar\nu$), while the zero-point energy of adsorption sites is negligible. The entropies of the free molecules (O_2, H_2, H_2O) were taken from taken from the standard tables in Physical Chemistry[10]. For those reactions involving the release of protons and electrons, the free energy of one pair of proton and electron ($H^+ + e^-$) was taken as $1/2G_{H2}$. The free energy of O_2(g) was derived as $G_{O2} = 2G_{H2O} - 2G_{H2} + 4.92$ eV since O_2 in triplet ground state is notoriously poorly described by DFT calculations. All the E_{ZPE} and S results can be obtained from the reference[11] and are shown in Table S8.

In the aqueous solution, the OER process generally involves four-electron oxidation steps, which can be written as:

$$H_2O + * \rightarrow OH^* + H^+ + e^-$$

$$OH^* \rightarrow O^* + H^+ + e^-$$

$$O^* + H_2O \rightarrow OOH^* + H^+ + e^-$$

$$OOH^* \rightarrow * + O_2(g) + H^+ + e^-$$

Where * denotes the adsorption site, OH*, O* and OOH* denote the adsorbed intermediates.

Meanwhile, the HER process with two-electron pathways, including a fast ptoton/electron transfer step and a fast hydrogen release step, can be written as:

$$* + H^+ + e^- \rightarrow H^*$$

$$H^* + H^+ + e^- \rightarrow * + H_2(g)$$

Then, the free energy change for OER electrochemical steps can be expressed as:

$$\Delta G_1 = G_{OH^*} + 1/2G_{H_2} - G_{H_2O} - G^* - 0.059 \times \mathrm{pH} - eU$$

$$\Delta G_2 = G_{O^*} + 1/2G_{H_2} - G_{OH^*} - 0.059 \times \mathrm{pH} - eU$$

$$\Delta G_3 = G_{OOH^*} + 1/2G_{H_2} - G_{H_2O} - G_{O^*} - 0.059 \times \mathrm{pH} - eU$$

$$\Delta G_4 = 2G_{H_2O} + G^* - 3/2G_{H_2} - G_{OOH^*} + 4.92 - 0.059 \times \mathrm{pH} - eU$$

The free energy change for HER electrochemical step can be expressed as:

$$\Delta G_{H^*} = G_{H^*} - 1/2G_{H_2} - G^* + 0.059 \times \mathrm{pH} - eU$$

Where 0.059 × pH represents the free energy contribution due to the variations in H concentration, *eU* represents the effect of a potential bias on all states involving one electron or hole in the electrode by shifting the energy, and *U* is the electrode potential relative to the normal hydrogen electrode (NHE).

Table S1. Lattice constant a (Å), c (Å) of bulk $LiAlTe_2$ using PBE and different vdW functionals

System	*Method*	*a* (Å)	*c* (Å)
Bulk $LiAlTe_2$	PBE	4.377	7.676
	optB88	4.328	7.205
	PBE-D2	4.240	6.970
	PBE-D3-G	4.333	7.229
	PBE-D3-BJ	4.276	7.079
	optPBE	4.349	7.268
	revPBE	4.385	7.410
	Expt.[1]	4.481	7.096

Table S2. Calculated lattice constants (*a*), interlayer distances (*d*) total heights (*h*), formation energies (E_{form}) and exfoliation energies (E_{exf}) of the $LiMX_2$ bilayers.

Materials	*a* (Å)	*d* (Å)	*h* (Å)	E_{form} (eV/Å^2)	E_{exf} (eV/Å^2)
$LiAlS_2$	3.75	2.63	9.90	-23.24	34.42
$LiAlSe_2$	3.96	2.73	10.40	-22.91	32.01
$LiAlTe_2$	4.32	2.76	11.17	-22.76	29.97
$LiGaS_2$	3.79	2.61	9.96	-23.32	33.44
$LiGaSe_2$	3.99	2.65	10.36	-24.03	27.24
$LiGaTe_2$	4.33	2.60	11.06	-25.46	27.49
$LiInS_2$	3.98	2.59	10.39	-21.97	35.86
$LiInSe_2$	4.16	2.65	10.75	-22.91	28.50
$LiInTe_2$	4.49	2.75	11.37	-23.06	26.58

Table S3. Calculated lattice constants (a), bond lengths of Li-X, X-M, M-X (l), total heights (h) and cohesive energies (E_{coh}) of the $LiMX_2$ monolayers.

Materials	a	l_{Li-X}	l_{X-M}	L_{M-X}	h	E_{coh}
	(Å)	(Å)	(Å)	(Å)	(Å)	(eV/atom)
$LiAlS_2$	3.80	2.25	2.17	2.39	3.60	-1.42
$LiAlSe_2$	4.02	2.36	2.31	2.54	3.79	-1.03
$LiAlTe_2$	4.39	2.57	2.54	2.79	4.09	-0.58
$LiGaS_2$	3.84	2.26	2.22	2.42	3.64	-1.19
$LiGaSe_2$	4.05	2.37	2.35	2.57	3.80	-0.87
$LiGaTe_2$	4.41	2.57	2.56	2.80	4.11	-0.50
$LiInS_2$	4.03	2.35	2.42	2.58	3.87	-1.13
$LiInSe_2$	4.22	2.45	2.54	2.72	4.01	-0.87
$LiInTe_2$	4.56	2.64	2.74	2.94	4.24	-0.54

The cohesive energy of the $LiMX_2$ monolayers is defined as:

$$E_{coh} = (E_{total} - \sum_i n_i \mu_i) / \sum_i n_i,$$

where E_{total} and n_i represent total energy and the number of *i-th* atom of the $LiMX_2$ structure in one unit cell, μ_i is the chemical potential of *i-th* atom in its bulk crystal. The negative cohesive energies that vary from -0.50 to -1.42 eV/atom suggest the energetic stability of these $LiMX_2$ monolayers.

Table S4. Carrier effective masses (m^*), elastic modulus (C), deformation potential constants (E_d) and carrier mobility (μ) of the $LiMX_2$ bilayers.

Materials	Carrier Type	m^*/m_0	C(N/m)	E_d (eV)	μ $(cm^2V^{-1}s^{-1})$
$LiAlS_2$	Electrons (x)	0.25	44.74	-3.71	**2934. 38**
	Hole (x)	1.76	44.74	-7.39	**14. 88**
	Electrons (y)	0.25	44.56	-3.98	**2543. 83**
	Hole (y)	1.75	44.56	-7.11	**16. 02**
$LiAlSe_2$	Electrons (x)	0.19	40.77	-4.23	**3318.53**
	Hole (x)	1.57	40.77	-9.98	**8.32**
	Electrons (y)	0.19	40.82	-4.33	**3183.81**
	Hole (y)	1.57	40.82	-9.74	**8.79**
$LiAlTe_2$	Electrons (x)	0.15	36.88	-5.07	**2625. 05**
	Hole (x)	1.38	36.88	-10.07	**8. 19**
	Electrons (y)	0.15	37.34	-5.17	**2527. 00**
	Holes (y)	1.38	37.34	-9.36	**9. 72**
$LiGaS_2$	Electrons (x)	0.21	41.49	-4.79	**2208. 56**
	Hole (x)	1.93	41.49	-8.19	**9. 15**
	Electrons (y)	0.21	40.69	-4.79	**2162. 89**
	Holes (y)	1.92	40.69	-9.26	**7. 07**
$LiGaSe_2$	Electrons (x)	0.11	40.24	-5.09	**6592.38**
	Hole (x)	1.73	40.24	-8.63	**8.89**
	Electrons (y)	0.11	39.97	-5.18	**6285.52**
	Holes (y)	1.73	39.97	-8.45	**9.23**
$LiGaTe_2$	Electrons (x)	0.11	34.92	-5.51	**4018. 00**
	Hole (x)	1.65	34.92	-3.95	**34. 58**
	Electrons (y)	0.11	34.57	-5.42	**4113. 76**
	Holes (y)	1.65	34.57	-4.21	**30. 01**
$LiInS_2$	Electrons (x)	0.24	39.83	-2.879	**4184. 77**
	Hole (x)	2.10	39.83	-5.42	**15. 33**
	Electrons (y)	0.24	41.46	-2.71	**4950. 61**
	Holes (y)	2.10	41.46	-4.98	**18. 95**
$LiInSe_2$	Electrons (x)	0.17	39.15	-4.17	**3611. 24**
	Hole (x)	1.91	39.15	-5.42	**16. 93**
	Electrons (y)	0.17	39.54	-4.28	**3458. 23**
	Holes (y)	1.91	39.54	-5.16	**19. 51**
$LiInTe_2$	Electrons (x)	0.13	37.09	-5.40	**2792. 57**
	Hole (x)	1.72	37.09	-7.94	**7. 75**
	Electrons (y)	0.13	36.85	-5.29	**2892. 38**
	Holes (y)	1.72	36.85	-8.06	**7. 52**

Table S5. HSE band gaps E_g(HSE), energy differences between VBM (or CBM) and water oxidation (or hydrogen reduction) potentials ΔE_1 (or ΔE_2), potential differences between top and bottom surfaces ΔV and the solar-to-hydrogen conversion efficiencies η_{STH} for the $LiMX_2$ trilayers.

Materials	E_g(HSE)	ΔE_1	ΔE_2	ΔV	η_{STH}
	(eV)	(eV)	(eV)	(V)	(%)
$LiAlS_2$	0.66	1.06	3.20	4.84	18.98
$LiAlSe_2$	0.20	0.68	2.26	3.97	22.69
$LiAlTe_2$[a]	0.15	0.22	1.26	2.56	30.14
$LiGaS_2$	0.03	1.24	1.74	4.19	21.80
$LiGaSe_2$	--	0.64	1.32	3.25	26.16
$LiGaTe_2$[a]	--	0.32	0.76	2.45	31.53
$LiInS_2$	0.70	1.30	1.57	3.40	24.36
$LiInSe_2$	0.62	0.83	0.13	2.35	30.82
$LiInTe_2$	0.77	0.34	0.76	1.57	33.09

Table S6. Calculated HSE band gaps E_g(HSE), energy differences between VBM (or CBM) and water oxidation (or reduction) potentials ΔE_1 (or ΔE_2), potential differences between top and bottom surfaces ΔV, quasi-particle band gaps E_g(GW), exciton binding energies E_b, and the solar-to-hydrogen conversion efficiencies η_{STH} for the $LiMX_2$ monolayers.

Materials	E_g(HSE)	ΔE_1	ΔE_2	ΔV	E_g(GW)	E_b	η_{STH}
	(eV)	(eV)	(eV)	(V)	(eV)	(eV)	(%)
$LiAlS_2$	3.30	1.40	2.30	1.63	4.34	0.92	1.00[a]
$LiAlSe_2$	2.38	1.00	1.43	1.29	3.33	0.75	8.68[a]
$LiAlTe_2$	1.60	0.39	0.81	0.83	2.38	0.53	19.76[a]
$LiGaS_2$	2.39	1.55	1.26	1.66	3.38	0.77	8.40[a]
$LiGaSe_2$	1.60	1.07	0.57	1.28	2.40	0.58	23.61[a]
$LiGaTe_2$	0.89	0.39	1.67	0.89	1.55	0.37	36.02[a]
$LiInS_2$	2.35	1.59	0.64	1.11	3.22	0.78	9.32[a]
$LiInSe_2$	1.78	1.12	0.27	0.84	2.55	0.63	21.29[a]
$LiInTe_2$	1.32	0.49	0.12	0.52	2.05	0.47	29.72[a]

[a] These values will be reduced in the actual photocatalytic process due to partial recombination of the photogenerated carriers.

Table S7. Carrier effective masses (m^*), elastic modulus (C), deformation potential constants (E_d) and carrier mobility (μ) of the $LiMX_2$ monolayers.

Materials	Carrier Type	m^*/m_0	C(N/m)	E_d (eV)	μ $(cm^2V^{-1}s^{-1})$
$LiAlS_2$	Electrons (*x*)	0.25	22.31	-8.09	**309.63**
	Hole (*x*)	1.81	22.31	-7.56	**6.71**
	Electrons (*y*)	0.25	22.57	-8.11	**312.03**
	Hole (*y*)	1.69	22.57	-7.32	**7.79**
$LiAlSe_2$	Electrons (*x*)	0.18	20.50	-8.01	**474.94**
	Hole (*x*)	1.63	20.50	-7.71	**6.34**
	Electrons (*y*)	0.18	20.42	-8.06	**467.08**
	Hole (*y*)	1.63	20.42	-7.63	**6.45**
$LiAlTe_2$	Electrons (*x*)	0.15	19.81	-8.08	**588.00**
	Hole (*x*)	1.41	19.81	-9.39	**4.64**
	Electrons (y)	0.15	19.77	-8.11	**583.396**
	Holes (y)	1.41	19.77	-9.48	**4.55**
$LiGaS_2$	Electrons (*x*)	0.20	21.90	-8.34	**418.79**
	Hole (*x*)	1.99	21.90	-6.37	**7.31**
	Electrons (y)	0.20	21.83	-8.31	**419.78**
	Holes (y)	1.98	21.83	-6.64	**6.74**
$LiGaSe_2$	Electrons (*x*)	0.14	20.60	-7.57	**827.66**
	Hole (*x*)	1.73	20.60	-7.12	**6.54**
	Electrons (y)	0.14	20.55	-7.61	**816.25**
	Holes (y)	1.73	20.55	-7.00	**6.72**
$LiGaTe_2$	Electrons (*x*)	0.11	18.59	-6.98	**1354.95**
	Hole (*x*)	1.43	18.59	-6.56	**8.54**
	Electrons (y)	0.11	18.67	-6.86	**1407.04**
	Holes (y)	1.43	18.67	-6.36	**9.12**
$LiInS_2$	Electrons (*x*)	0.23	21.92	-5.52	**636.46**
	Hole (*x*)	2.03	21.92	-3.39	**22.49**
	Electrons (y)	0.23	21.75	-5.49	**638.00**
	Holes (y)	2.03	21.75	-3.55	**20.34**
$LiInSe_2$	Electrons (*x*)	0.18	20.39	-5.76	**885.18**
	Hole (*x*)	1.80	20.39	-4.52	**13.57**
	Electrons (y)	0.18	20.71	-5.65	**933.74**
	Holes (y)	1.80	20.71	-4.01	**17.55**
$LiInTe_2$	Electrons (*x*)	0.12	19.56	-6.22	**1382.57**
	Hole (*x*)	1.44	19.56	-5.78	**10.67**
	Electrons (y)	0.12	19.53	-6.19	**1397.54**
	Holes (y)	1.44	19.53	-5.07	**13.86**

Table S8. Values used for the entropy and zero-point energy corrections in determining the free energy of reactants, products, and intermediate species adsorbed on catalysts[11]. For the adsorbates, the ZPE values are averaged over all single atom catalyst systems since they have rather close value.

Species	**T ×S (eV) (298K)**	**ZPE (eV)**
H^*	0	0.17
O^*	0	0.07
OH^*	0	0.33
OOH^*	0	0.43
$H_2(g)$	0.41	0.27
$H_2O(g)$	0.58	0.57

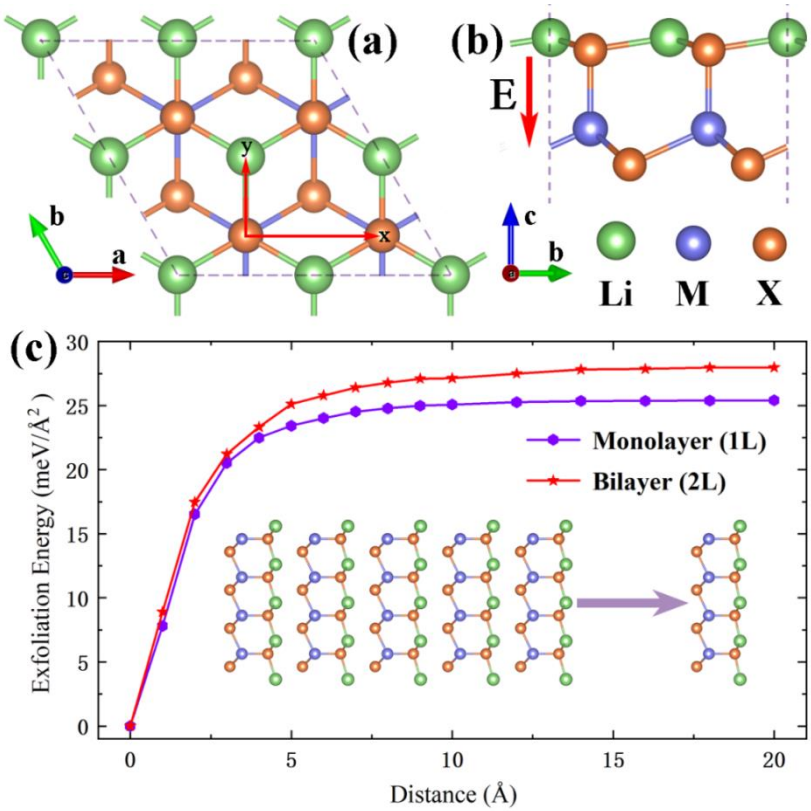

Figure S1. (a) Top and side views of the atomic structures of $LiMX_2$ monolayer. The red arrows indicate the directions of the vertical electric field. (c) Exfoliation energy vs. separation distance for $LiAlTe_2$ monolayer and bilayer.

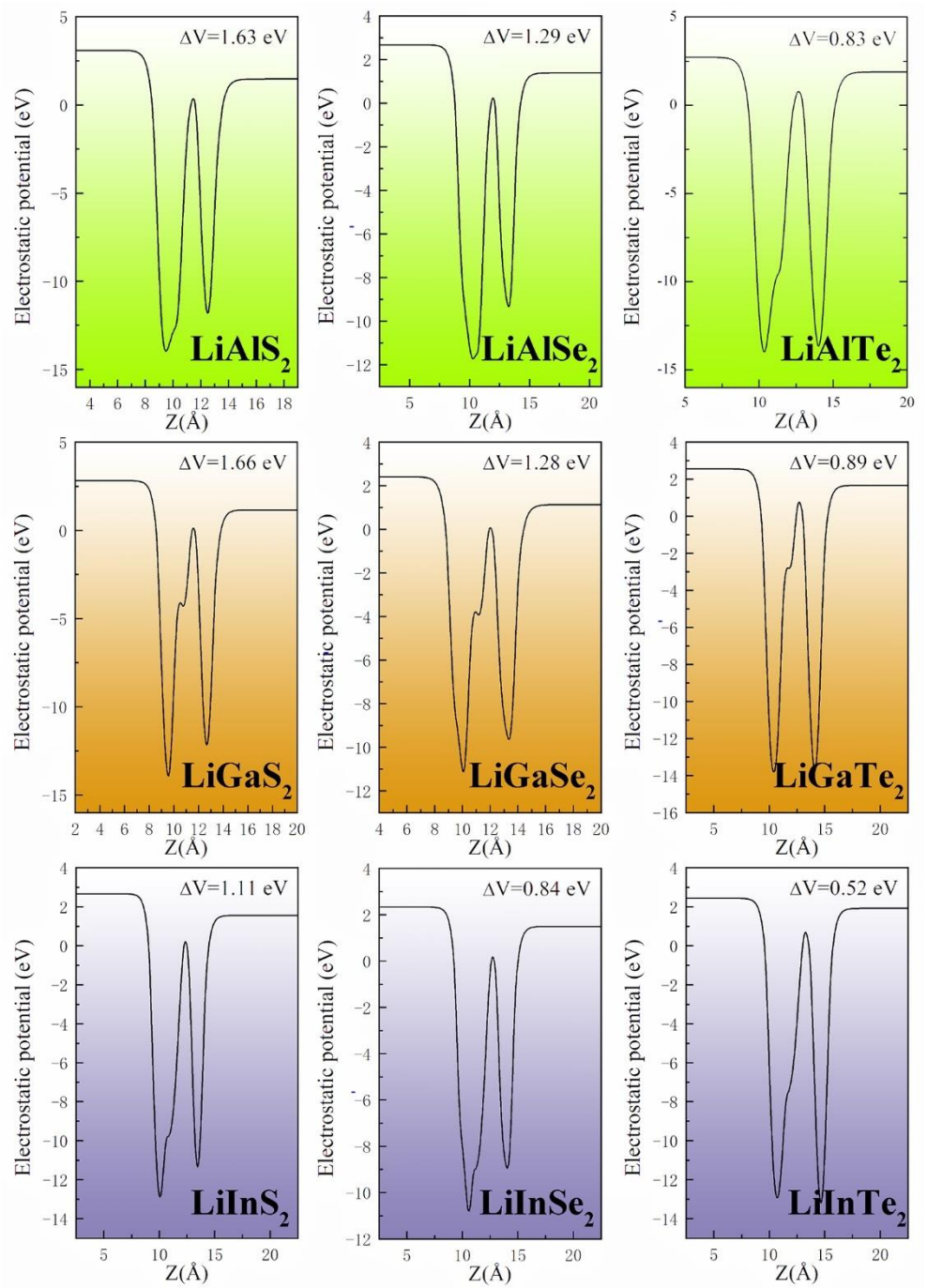

Figure S2. Plane-averaged electrostatic potential differences of the $LiMX_2$ monolayers.

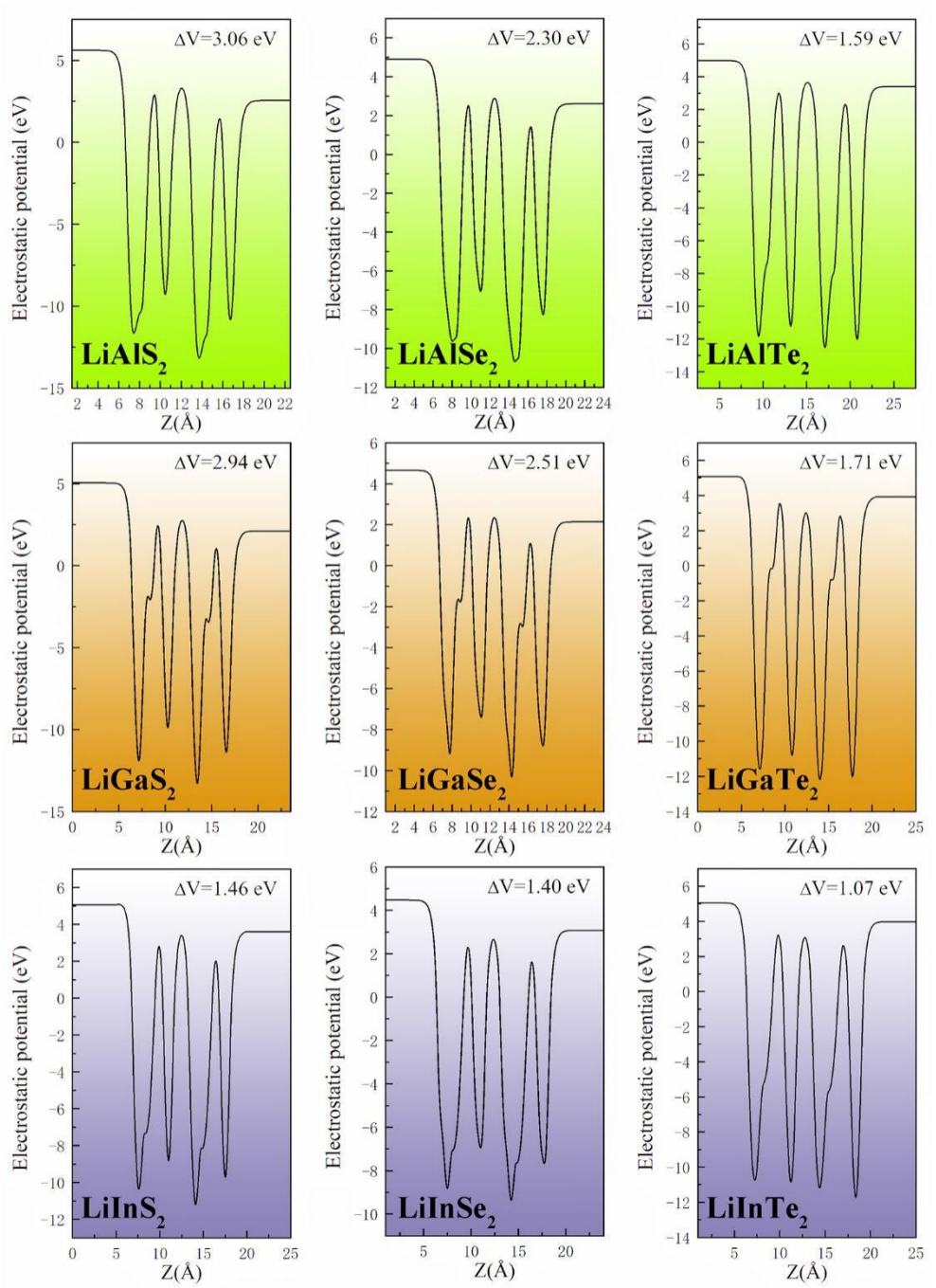

Figure S3. Plane-averaged electrostatic potential differences of the $LiMX_2$ bilayers.

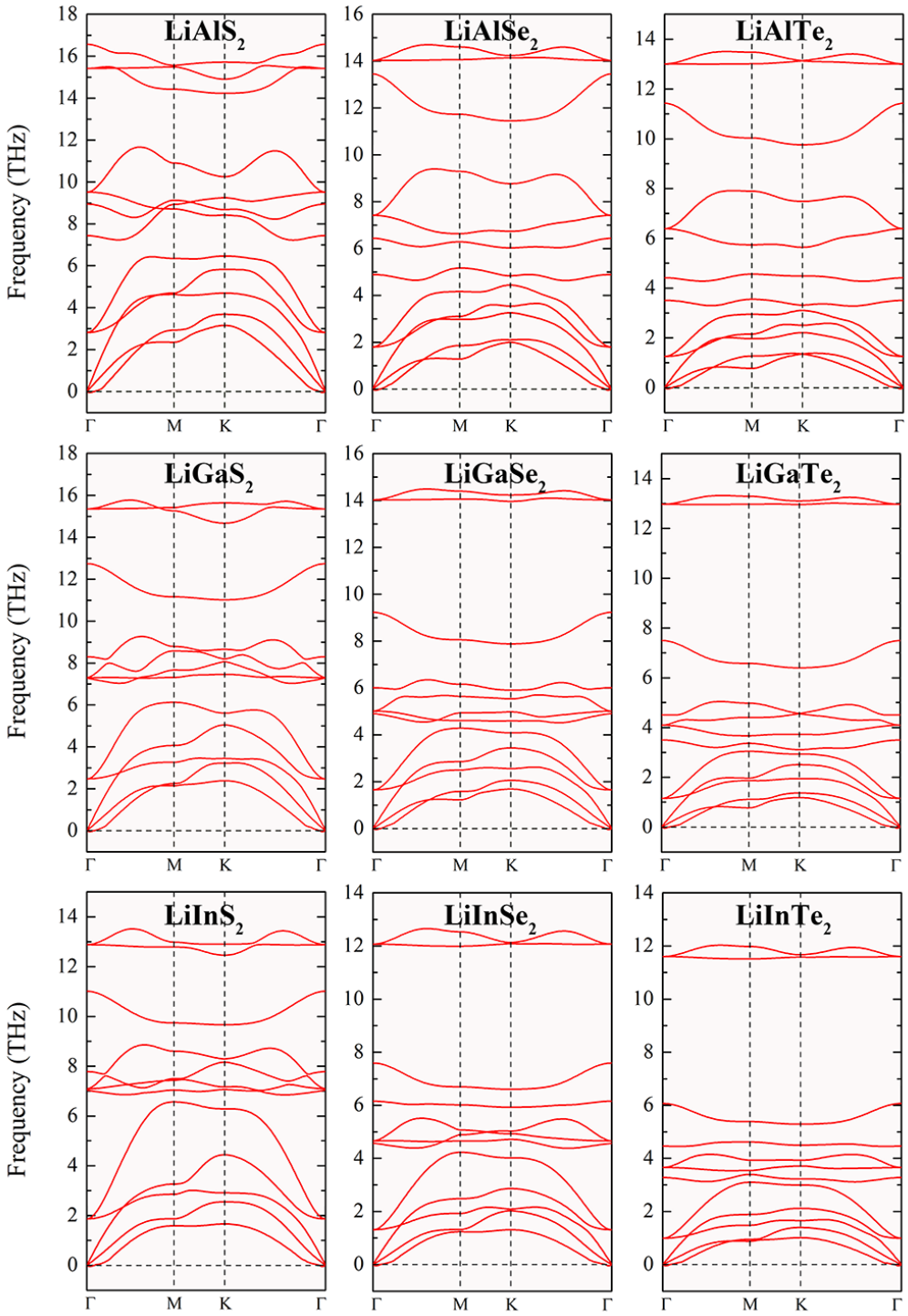

Figure S4. Phonon band diagrams of the $LiMX_2$ monolayers.

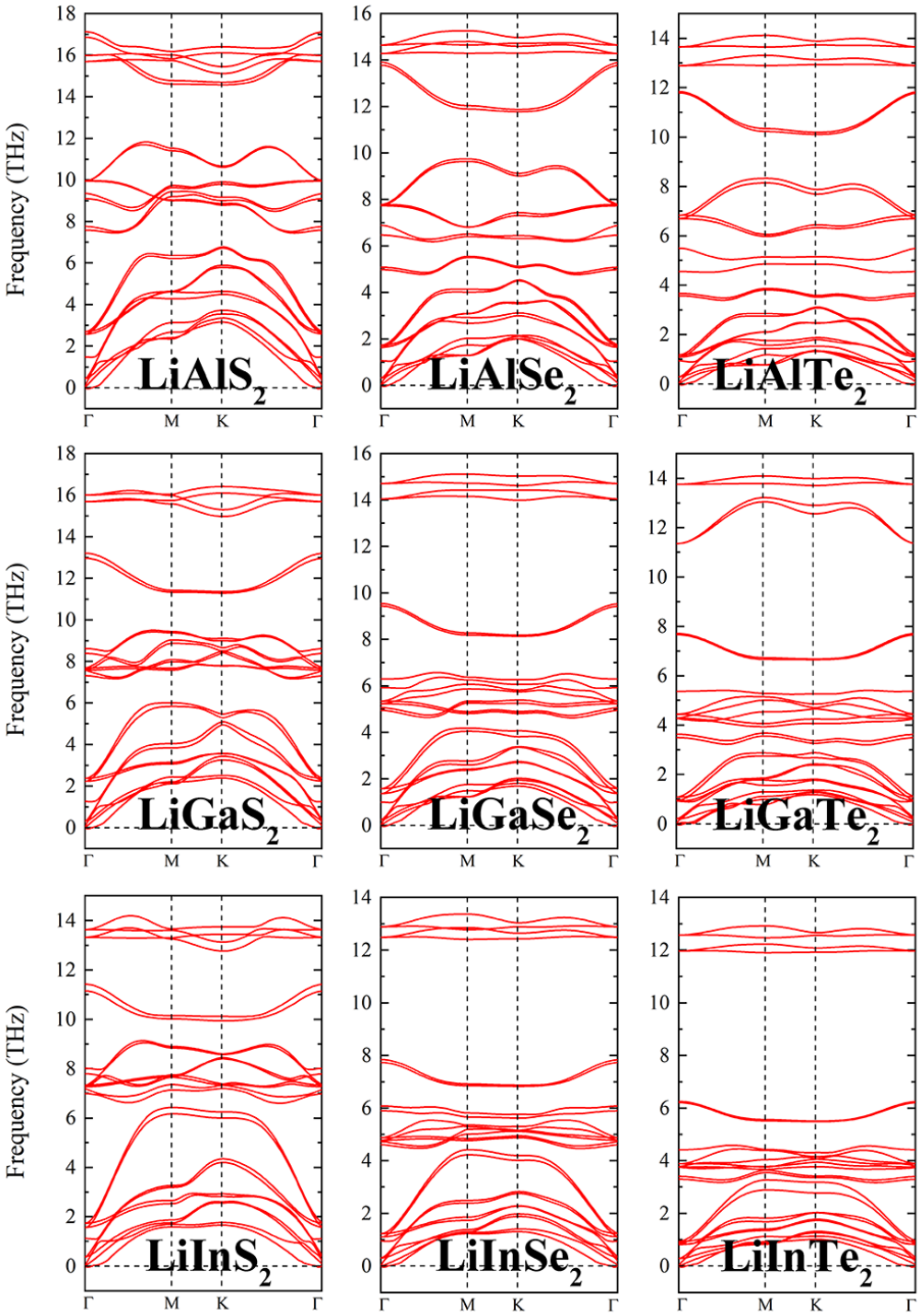

Figure S5. Phonon band diagrams of the $LiMX_2$ bilayers.

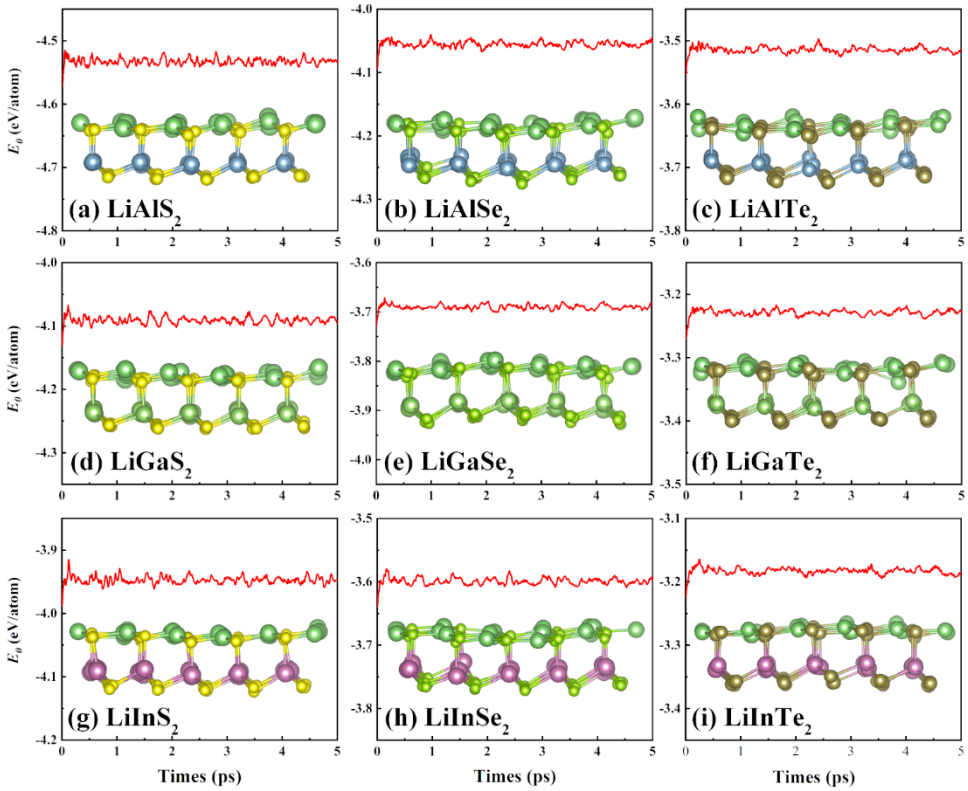

Figure S6. Evolution of total energies per atom of $LiMX_2$ monolayers in 5×5 supercells obtained from 5 ps AIMD simulations. The final conformations at t = 5 ps are shown in the insets.

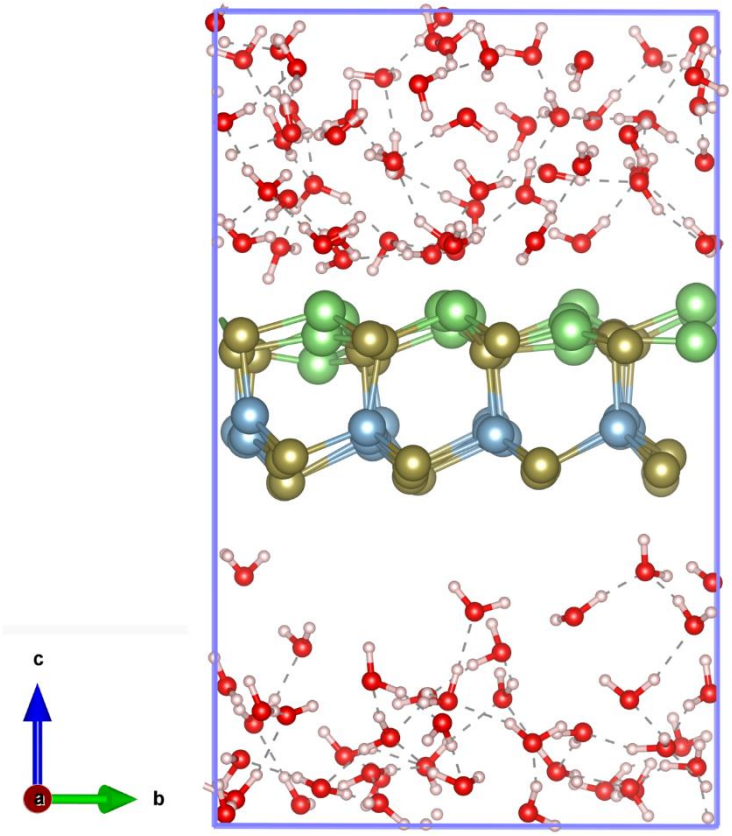

Figure S7. The final conformation of the $LiAlTe_2$ monolayer in liquid water after annealing at 300 K for 5 ps.

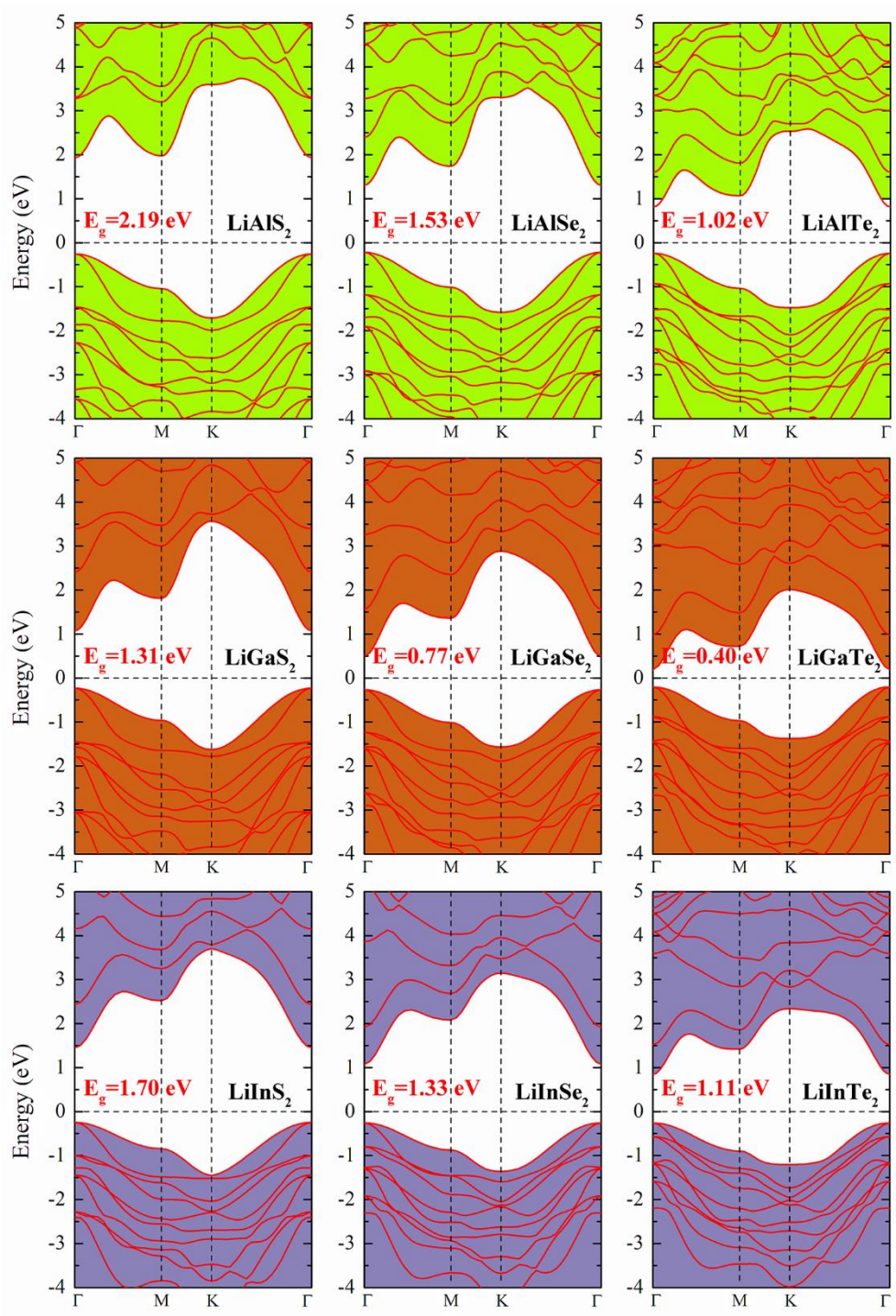

Figure S8. Band structures of the $LiMX_2$ bilayers calculated with the HSE06 functional. The fermi levels are set to 0 eV.

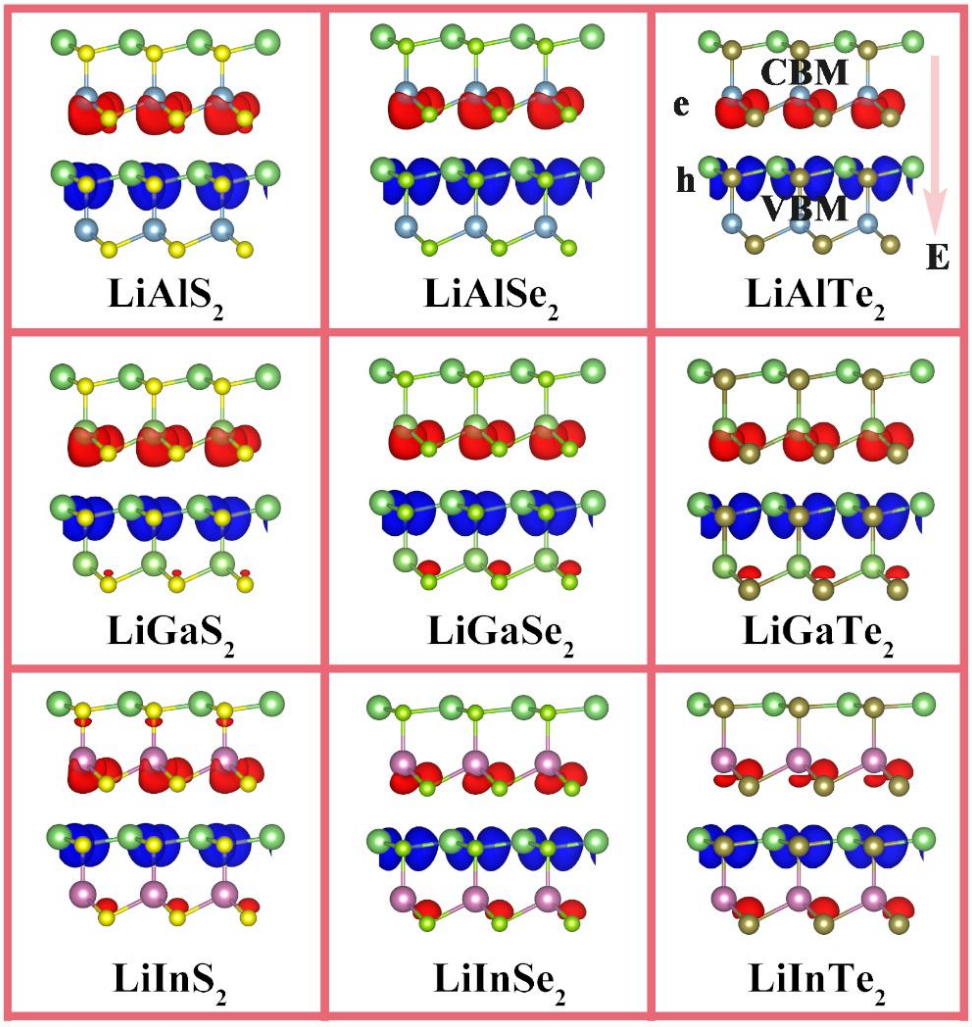

Figure S9. Partial charge densities of VBM and CBM for the $LiMX_2$ bilayers. The blue and red regions indicate the distributions of the VBM and CBM, respectively. The isosurface value is 0.007 e $Å^{-3}$.

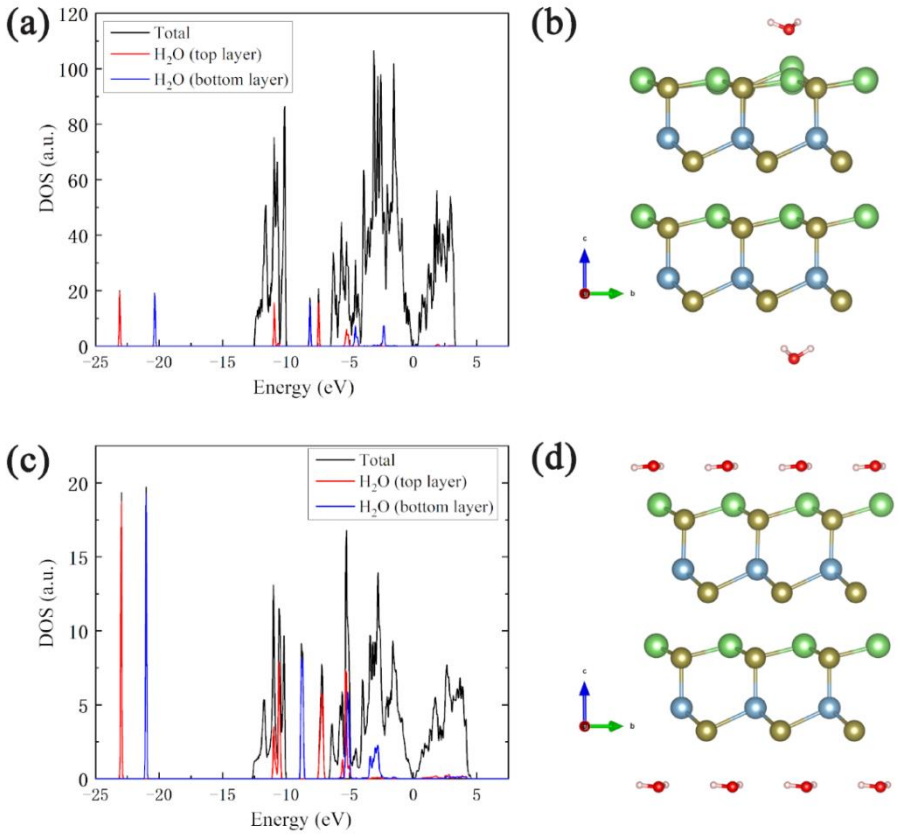

Figure S10. (a) The total DOS for H_2O@$LiAlTe_2$ bilayer, and the projected DOS for a H_2O molecule adsorbed on top layer and bottom layer, respectively. (b) The atomic structure of H_2O@$LiAlTe_2$ bilayer for a H_2O molecule adsorbed on the top layer and bottom layer of $LiAlTe_2$ bilayer respectively. (c) The total DOS for H_2O@$LiAlTe_2$ bilayer, and the projected DOS for H_2O molecule layer adsorbed on top layer and bottom layer, respectively. (d) The atomic structure of H_2O@$LiAlTe_2$ bilayer for H_2O molecule layer adsorbed on the top layer and bottom layer of $LiAlTe_2$ bilayer respectively.

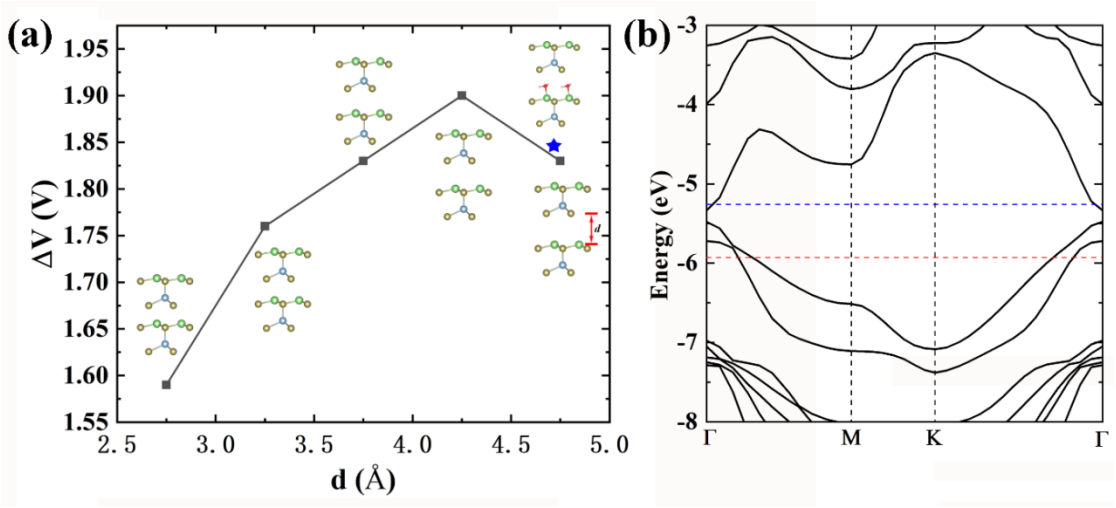

Figure S11. (a) The vacuum levels difference (ΔV) vs. interlayer distance (d) for $LiAlTe_2$ bilayer. The blue star represents the situation that the water molecules intercalate into the interlayer of the $LiAlTe_2$ bilayer. (b) The band structure of the $LiAlTe_2$ bilayer with the water molecules intercalate into the interlayer space calculated with the HSE06 functional. All the energy positions are relative to the vacuum levels. The energy of the vacuum level on the bottom side was set to zero. The dotted red and blue lines represent the hydrogen reduction potential (H^+/H_2) and the water oxidation potential of (H_2O/O_2) at pH = 7, respectively.

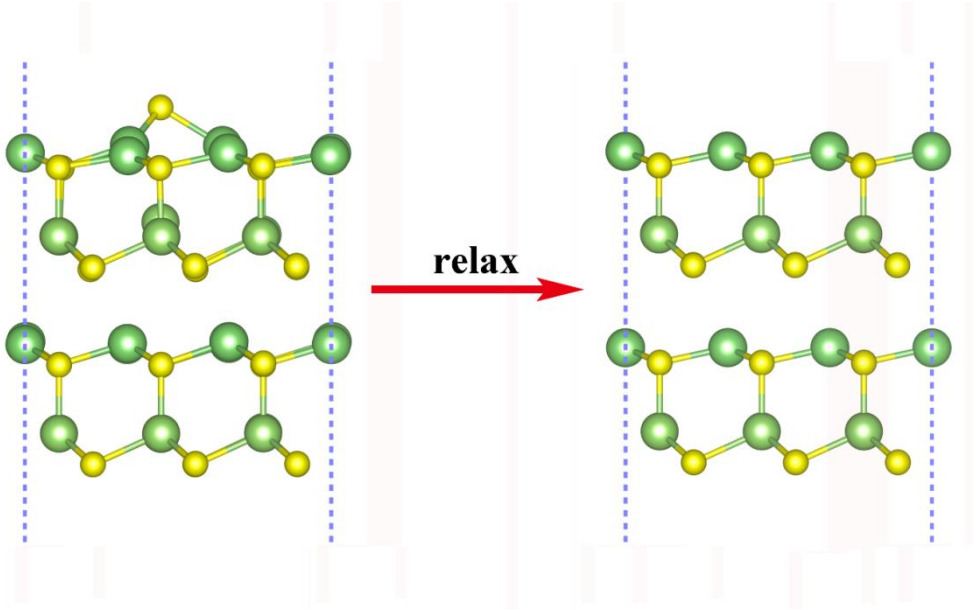

Figure S12. The geometry structures of $LiAlTe_2$ bilayer before and after the desorption of H atom.

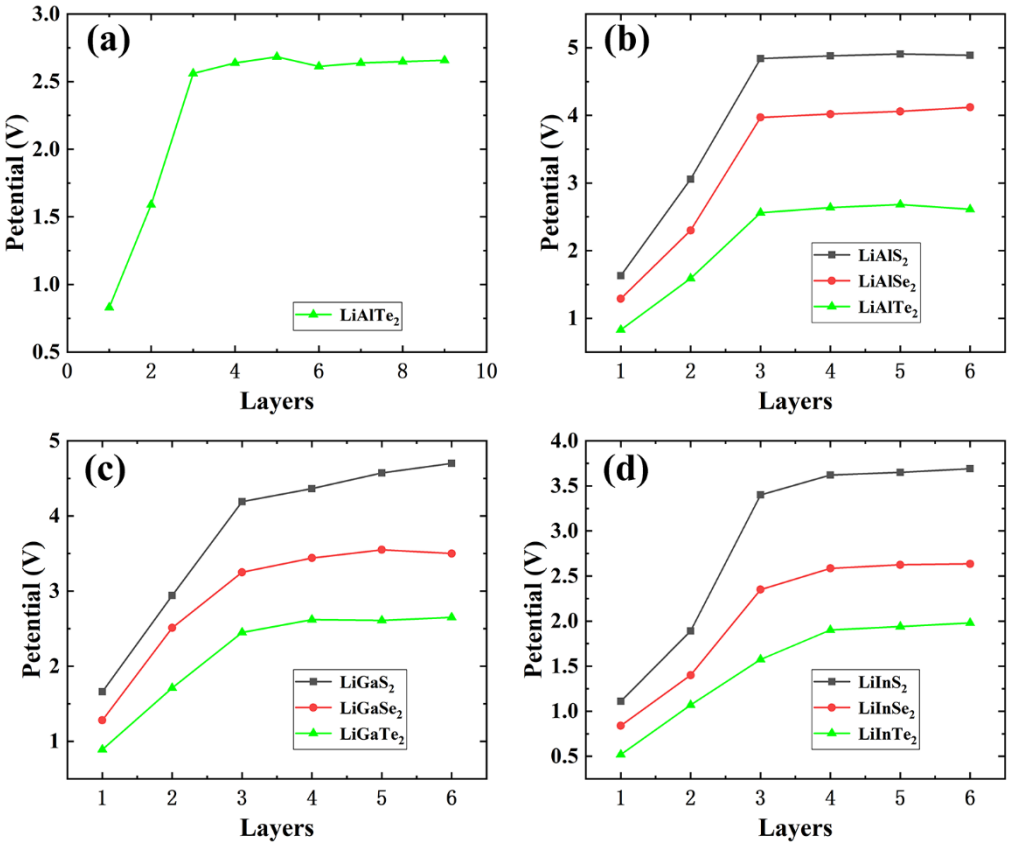

Figure S13. Variations of vacuum levels differences (ΔV) as functions of thickness for the $LiMX_2$ layers.

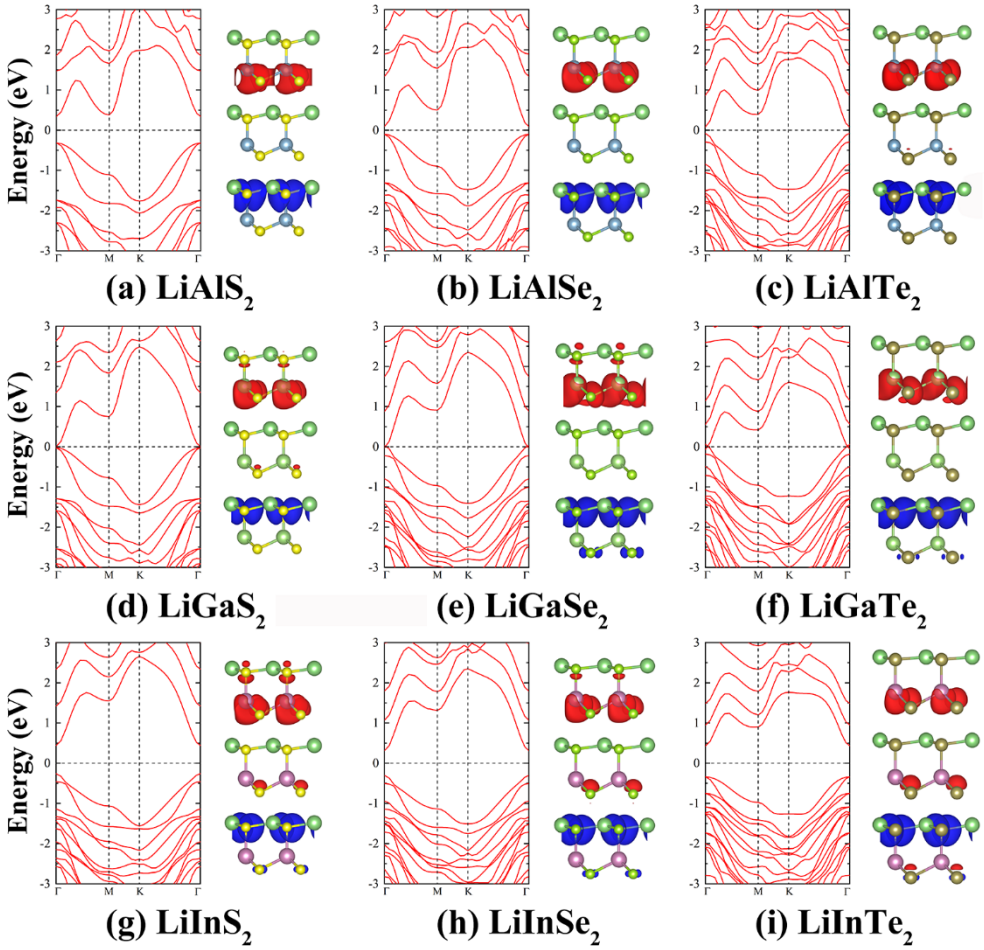

Figure S14. Band structures (HSE06) and partial charge densities of VBM and CBM for the $LiMX_2$ trilayers. The blue and red regions indicate the distributions of VBM and CBM, respectively. The isosurface value is 0.005 e $Å^{-3}$.

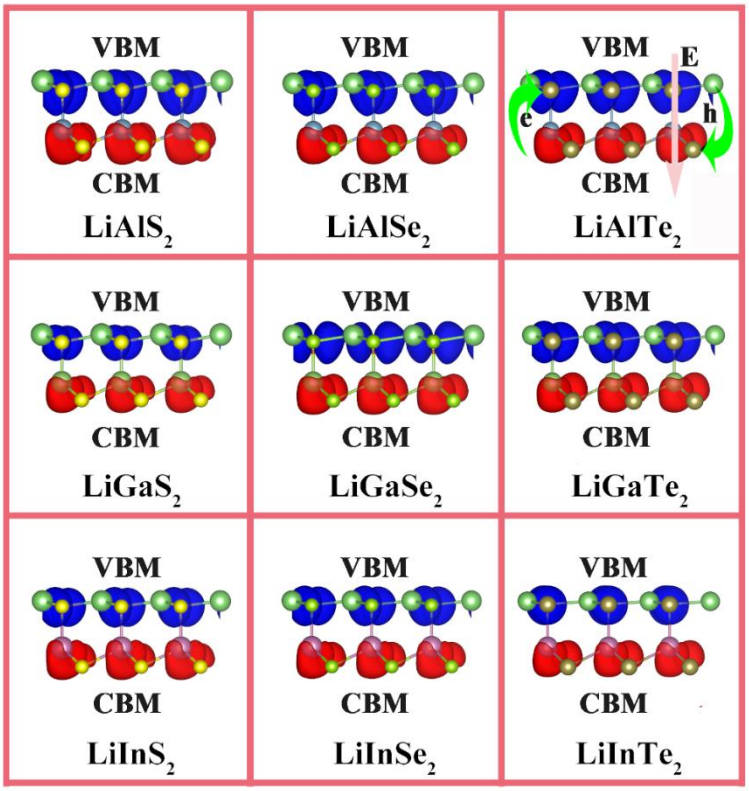

Figure S15. Partial charge densities of VBM and CBM for the $LiMX_2$ monolayers. The blue and red regions indicate the distributions of VBM and CBM, respectively. The isosurface value is 0.007 e $Å^{-3}$.

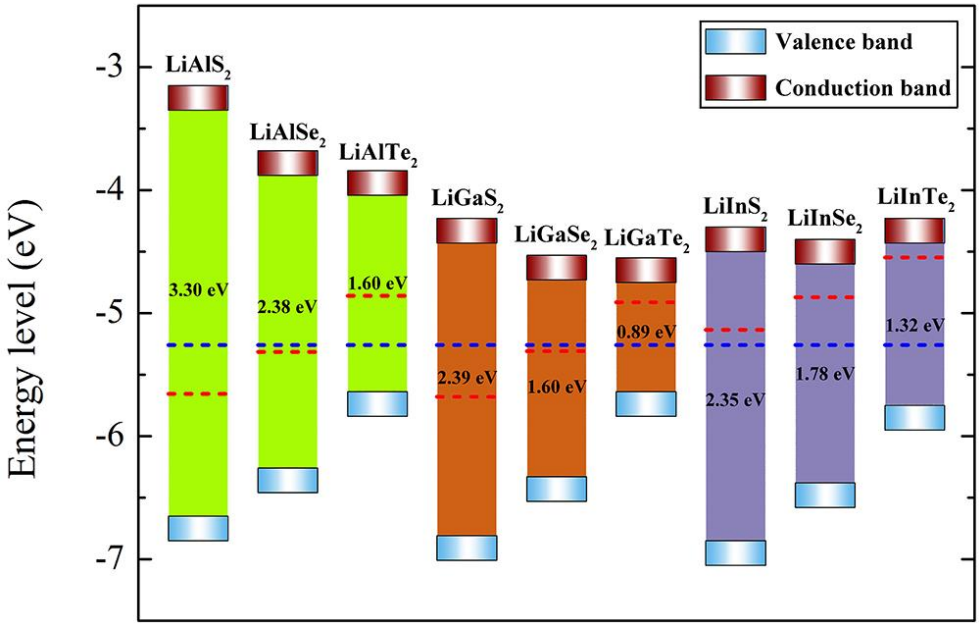

Figure S16. Band edge positions of the $LiMX_2$ monolayers relative to the vacuum levels. The energy of the vacuum level on the bottom side was set to zero. The dotted red and blue lines represent the reduction potential of H^+/H_2 and the oxidation potential of H_2O/O_2 at pH = 7, respectively.

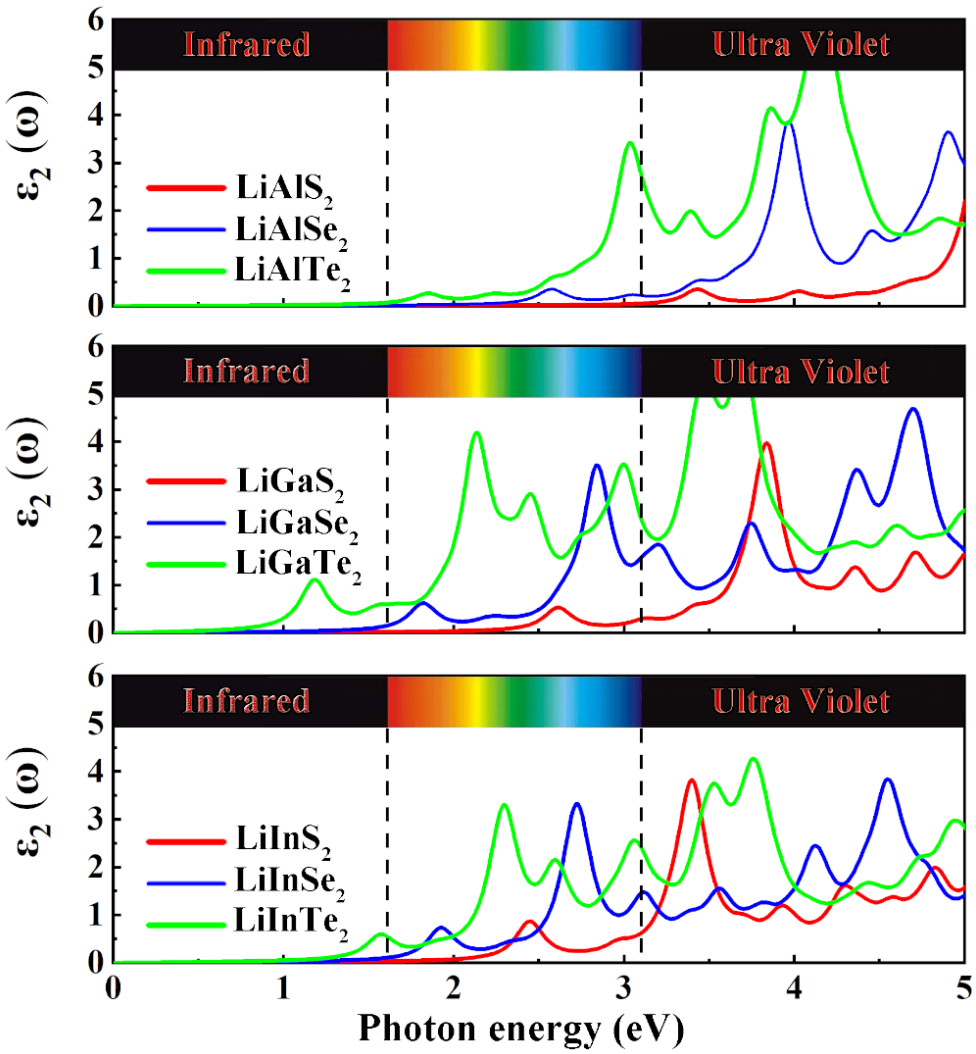

Figure S17. The calculated absorption spectrum of the $LiMX_2$ monolayers by GW+BSE.

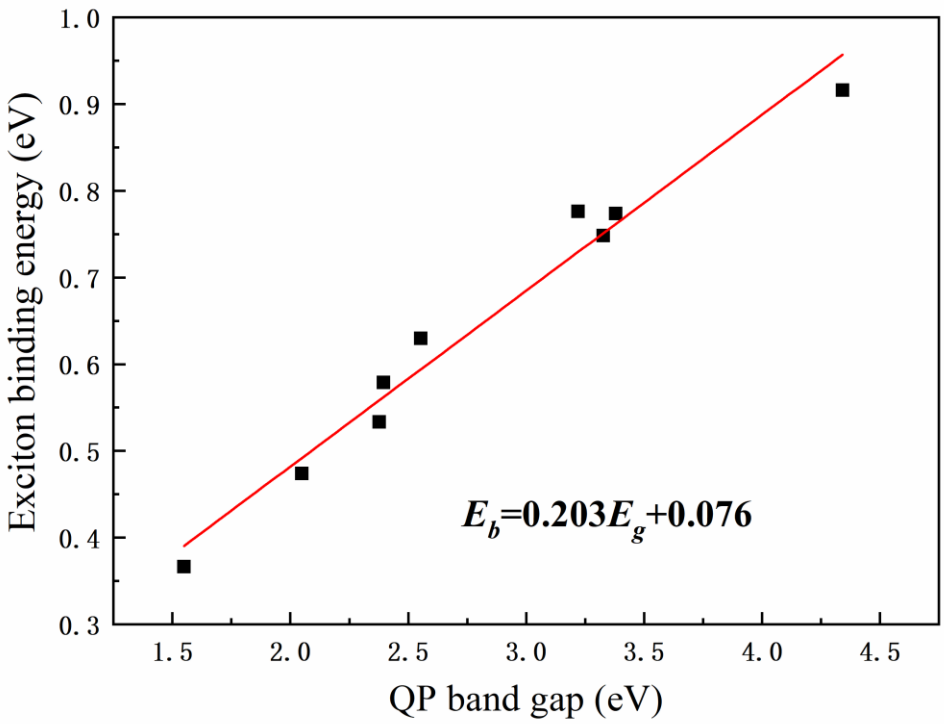

Figure S18. The exciton binding energy (E_b) versus the direct QP band gap (E_g) for $LiMX_2$ monolayers.

References

1. C. F. Fu, J. Sun, Q. Luo, X. Li, W. Hu and J. Yang, *Nano Lett.*, 2018, **18**, 6312-6317.
2. J. Yang, D. Wang, H. Han and C. Li, *Acc. Chem. Res.*, 2013, **46**, 1900-1909.
3. C. C. McCrory, S. Jung, I. M. Ferrer, S. M. Chatman, J. C. Peters and T. F. Jaramillo, *J. Am. Chem. Soc.*, 2015, **137**, 4347-4357.
4. Y. Zheng, Y. Jiao, M. Jaroniec and S. Z. Qiao, *Angew. Chem., Int. Ed.*, 2015, **54**, 52-65.
5. J. Qiao, X. Kong, Z. X. Hu, F. Yang and W. Ji, *Nat. Commun.*, 2014, **5**, 4475.
6. J. Rossmeisl, Z. W. Qu, H. Zhu, G. J. Kroes and J. K. Nørskov, *J. Electroanal. Chem.*, 2007, **607**, 83-89.
7. J. K. Nørskov, J. Rossmeisl, A. Logadottir and L. Lindqvist, *J. Phys. Chem. B*, 2004, **108**, 17886-17892.
8. J. Greeley, T. F. Jaramillo, J. Bonde, I. B. Chorkendorff and J. K. Norskov, *Nat. Mater.*, 2006, **5**, 909-913.
9. A. Valdés, Z.-W. Qu and G.-J. Kroes, *J. Phys. Chem. C*, 2008, **112**, 9872-9879.
10. De Paula J. Atkins' Physical Chemistry (Oxford University Press, Oxford, 2010)
11. H. X. Xu, D. J. Cheng, D. P. Cao and X. C. Zeng, *Nat. Catal.*, 2018, **1**, 339-348.